Asociación Argentina
de Mecánica Computacional

Mecánica Computacional Vol XXXII, págs. 1271-1295 (artículo completo)
Carlos G. García Garino, Aníbal E. Mirasso, Mario A. Storti, Miguel E. Tornello (Eds.)
Mendoza, Argentina, 19-22 Noviembre 2013

# POLLUTANT DISPERSION SIMULATION IN STREET CANYONS USING THE FINITE ELEMENT METHOD AND SHARED MEMORY PARALLELIZATION

**Deborah M. S. Madalozzo, Alexandre L. Braun and Armando M. Awruch**

*PPGEC/UFRGS, Graduate Program in Civil Engineering, Federal University of Rio Grande do Sul, Av. Osvaldo Aranha 99, 90035-190, Porto Alegre – RS, Brazil,*
*http://www.ufrgs.br/engcivil/ppgec/*

**Keywords:** Computational Fluid Dynamics (CFD), Finite Element Method (FEM), Pollutant Dispersion, Non-Isothermal Flow, Large Eddy Simulation (LES).

**Abstract**. Air pollution generated by vehicles with internal combustion engines is one of the biggest problems the large cities are facing today. Therefore, the development of numerical techniques for evaluating and controlling the levels of pollutants is essential to maintain the urban environment balance. In the central regions of large cities, the so-called street canyons represent the basic geometric unit, where significant changes can be observed in the wind flow and pollutant dispersion as function of thermal conditions and geometrical configuration of the canyons. In this way, a numerical model based on CFD techniques is proposed in this work to simulate incompressible flows considering heat and mass transfer phenomena. In the present model, an explicit two-step Taylor-Galerkin scheme is adopted where the spatial discretization is performed using the finite element method (FEM) with eight-node hexahedral elements, one-point quadrature and hourglass control techniques. The pressure field is explicitly obtained by using the pseudo-compressibility hypothesis and the velocity and temperature fields are coupled by buoyancy forces according to the Boussinesq approximation. Large eddy simulation (LES) is utilized to analyze turbulent flows, where the sub-grid scales are modeled using both, the classical Smagorinsky`s model and the dynamic model. Programming techniques for shared memory parallelization are also utilized in order to improve the performance of the present numerical code. Pollutant dispersion problems are simulated considering different geometrical and thermal configurations in order to adequately characterize the conditions encountered in urban areas.

## 1 INTRODUCTION

The environmental conditions in large cities have been constantly deteriorated during the last decades owing to pollutants emitted by motor vehicles. Government agencies for air pollution control have adopted some procedures in order to reduce the pollutant emissions, which are mainly based on data obtained from monitoring stations strategically located to quantify the air quality in terms of pollutant concentration. However, the number of monitoring stations is clearly insufficient to describe the distribution of pollutants over the streets accurately.

The flow field in street canyons is mainly influenced by geometrical and meteorological aspects such as building shape, street width, wind speed and direction, turbulence, solar radiation and photochemical reactions (see Kim and Baik, 1999). Some comprehensive reviews on street canyon flows may be found in Vardoulakis et al. (2003); Ahmad et al. (2005); Li et al. (2006) and Hajra (2011). Experimental analyses of the flow field inside street canyons for different aspect ratios (AR = building height/street width) were performed by Oke (1988), while numerical investigations may be found in Lee and Park (1994); Sini et al. (1996); Baik and Kim (1999); Chan et al. (2002) and Jeong and Andrews (2002), where two-dimensional models were adopted.

In order to reproduce the street canyon problem realistically, street intersections must be also considered. Complicated flow patterns are observed at the intersection region, where dispersion and mixing of pollutants are strongly influenced by the geometric configuration of the street intersections (see Chan et al., 2003; Yassin et al., 2008 and Soulhac et al., 2009). In the numerical studies performed so far, pollutant dispersion through street canyons has been determined considering only passive pollutants, where chemical reactions are not included in the transport equations.

Building walls and street surfaces composing the urban canyon are heated owing to the incidence of solar radiation, which leads to the development of upward buoyancy forces over the flow field. Parameters influencing solar heating in street canyons are orientation, albedo, emissivity of the building and street materials, and the sky view factor. Kim and Baik (1999); Sini et al. (1996); Xie et al. (2005); Xie et al. (2006); Baik et al. (2003); Li et al. (2009) and Cheng and Liu (2011) analyzed the influence of wall temperature in the flow structure and the vertical transport.

A numerical model based on the Finite Element Method (FEM) and Large Eddy Simulation (LES) in order to investigate pollutant dispersion in street canyons with thermal effects is proposed in this work. The basic formulation employed in the present model was previously validated on building aerodynamics applications by Braun and Awruch (2009), which is extended here to include mass and heat transport phenomena in the flow analysis. In order to verify the relevance of the modeling dimensionality in a pollutant dispersion investigation, two numerical applications were studied considering two and three-dimensional models. In the first numerical application presented, a realistic problem was proposed where an urban region was reproduced considering a typical geometric configuration of buildings and street canyons found in large cities. In the second application, a three-dimensional street canyon problem was reproduced.

## 2 MODEL DESCRIPTION

### 2.1 Flow and transport equations

The flow problem in urban street canyons is mathematically described using balance

equations for momentum, mass and energy, and the scalar transport equation for pollutant species. Some hypothesis may be considered in order to simply the general formulation. In the present work, the same assumptions adopted by Braun and Awruch (2009) to characterize wind flows are utilized and additional hypotheses are also specified regarding the pollutant transport. The main postulates assumed in the present model may be summarized as follows:

(a) Wind flows are assumed to be incompressible;

(b) Air density is assumed to be constant;

(c) Air density variations due to temperature effects are considered only in terms of buoyancy forces acting on the momentum equations;

(d) Pollutant species are assumed to be mechanically passive and chemically inert;

(e) The Newtonian fluid model is adopted for constitutive description of the air.

The governing equations are kinematically described using the classical Eulerian approach and the mass balance equation is written here according to the pseudo-compressibility hypothesis (see Braun and Awruch, 2009A), which leads to flow formulations where the pressure field is obtained explicitly. Considering the Cartesian coordinate system, the flow governing equations for street canyon flows may be presented as follows:

*Momentum equations – the Navier-Stokes equations:*

$$\frac{\partial v_i}{\partial t} + v_j \frac{\partial v_i}{\partial x_j} = \frac{\partial}{\partial x_j}\left[ \nu \left( \frac{\partial v_i}{\partial x_j} + \frac{\partial v_j}{\partial x_i} \right) + \frac{\lambda}{\rho} \frac{\partial v_k}{\partial x_k} \delta_{ij} \right] + \frac{1}{\rho}\left( S_i - \frac{\partial p}{\partial x_i} \right) \qquad (\mathrm{i,j} = 1,2,3) \ \text{in } \Omega \quad (1)$$

*Mass conservation equation – the pseudo-compressibility form:*

$$\frac{\partial p}{\partial t} + v_j \frac{\partial p}{\partial x_j} + \rho c_s^2 \frac{\partial v_j}{\partial x_j} = 0 \qquad (\mathrm{j} = 1,2,3) \qquad \text{in } \Omega \qquad (2)$$

*Energy conservation equation:*

$$\frac{\partial T}{\partial t} + v_j \frac{\partial T}{\partial x_j} = \frac{1}{\rho c_v}\left( k \frac{\partial^2 T}{\partial x_j^2} + \rho S_T \right) \qquad (\mathrm{j} = 1,2,3) \qquad \text{in } \Omega \qquad (3)$$

*Pollutant transport equation:*

$$\frac{\partial C}{\partial t} + v_j \frac{\partial C}{\partial x_j} = D \frac{\partial^2 C}{\partial x_j^2} + S_P \qquad (\mathrm{j} = 1,2,3) \qquad \text{in } \Omega \qquad (4)$$

where $v_i$ and $S_\mathrm{i}$ are components of the vectors of flow velocity and body force, respectively, which are given according to the direction of the Cartesian axes $x_i$, $p$ is the thermodynamic pressure, $T$ is the temperature, $C$ is the pollutant concentration and $\delta_\mathrm{ij}$ denotes the components of the Kroenecker's delta ($\delta_\mathrm{ij} = 1$ for $i = j$; $\delta_\mathrm{ij} = 0$ for $i \neq j$). The source terms for temperature and pollutant are denoted by $S_T$ and $S_P$, respectively. The fluid properties are given by the fluid specific mass $\rho$, the kinematic viscosity $\nu$, the bulk viscosity $\lambda$, the constant of isotropic thermal conductivity $k$, the constant of isotropic pollutant diffusion $D$, the specific heat at constant volume $c_v$ and the sound speed in the flow field $c_s$. The governing equations are valid for a spatial domain $\Omega$ and a time interval $[t_0, t]$, where $t_0$ is the initial time, when initial conditions for the flow variables must be defined. In order to solve the system of governing

equations, essential and natural boundary conditions for the flow variables must be also imposed over the spatial domain where the problem takes place.

Incompressible flows under thermal effects are generally analyzed using the Boussinesq's approximation, where density variations are considered in terms of body forces. By including effects of concentration, a general buoyancy force may be described as follows:

$$S_i = -\rho g_i \left[ \beta (T - T_0) + \beta_C (C - C_0) \right] \tag{5}$$

where $\beta$ is the coefficient of volumetric expansion due to thermal effects, $\beta_C$ is the coefficient of volumetric expansion due to concentration variation, $g_i$ are the components of the vector of gravity acceleration **g**, which are given according to the direction of the Cartesian axes $x_i$, and $T_0$ and $C_0$ are reference values for temperature and concentration, which are usually associated with undisturbed regions of the flow field. In the present work, the influence of concentration variations over the fluctuating gravitational forces (Eq. 5) is disregarded.

## 2.2 Turbulence modeling – LES

The main advantage of LES over turbulence models based on the RANS equations is related to the range of turbulence scales modeled. While RANS schemes try to model the full range of the energy spectrum and, consequently, all the turbulence scales, LES models are only concerned with scales below the size of a specified spatial filter, which is usually associated with the size of the finite elements for algorithms based on the FEM, whereas the turbulence scales above the filter size are solved directly. The basic step in the LES approach is the spatial filtering procedure performed over the flow variables, which are decomposed into components referring to large and sub-grid scales. Considering a general flow variable denoted by $\phi$, the filtering operation can be mathematically described as the convolution of $\phi$ with a kernel $G$ representing the filter function, that is:

$$\overline{\phi}\left(x_i, t\right) = \int_{\Omega} \phi\left(r_i, t\right) G\left(x_i - r_i, t\right) dr_i \tag{6}$$

where $\overline{\phi}$ is the large scale component of $\phi$, such that $\phi = \overline{\phi} + \phi'$, where $\phi'$ is the SGS component of $\phi$. The spatial field where the filtering operation takes place is indicated by $\Omega$. For a box filter, the kernel function is defined by:

$$G\left(x_i - r_i, t\right) = \begin{cases} \displaystyle\prod_{i=1}^{n} \frac{1}{\overline{\Delta}_i} & \text{if } \left|x_i - r_i\right| \le \dfrac{\overline{\Delta}_i}{2} \\ 0 & \text{if } \left|x_i - r_i\right| > \dfrac{\overline{\Delta}_i}{2} \end{cases} \qquad (\text{i} = 1,\text{n}) \tag{7}$$

where $\overline{\Delta}_i$ is the filter width in the $i$-th Cartesian direction and $n$ is the number of dimensions of the filter operator.

By applying the filtering procedure (Eq. 6) over the flow governing equations (Eqs. 1-4), the advective terms lead to the SGS terms. The term involving SGS interactions in the momentum equations is referred to as SGS Reynolds stress tensor, which is usually defined as:

$$\sigma_{ij}^{SGS} = \rho \overline{v_i' v_j'} \tag{8}$$

In order to close the mathematical problem, the deviatoric part of the SGS Reynolds stress tensor is approximated using the Boussinesq eddy viscosity model as follows:

$$\tau_{ij}^{SGS} = \sigma_{ij}^{SGS} - \frac{1}{3}\sigma_{kk}^{SGS}\delta_{ij} = \sigma_{ij}^{SGS} - \frac{2}{3}\overline{E}_k\delta_{ij} \qquad \Rightarrow \qquad \tau_{ij}^{SGS} = -2\nu_t\overline{S}_{ij} \tag{9}$$

where $\overline{E}_k$ is the SGS turbulent kinetic energy, $\nu_t$ is the kinematic eddy viscosity and $\overline{S}_{ij}$ are the components of the strain rate tensor defined in terms of the large scale velocity field. The SGS terms in the heat and pollutant transport equations denote SGS turbulent fluxes of heat and pollutant, respectively, which may be written as:

$$-c_v\overline{v_j'T'} = k_t\frac{\partial\overline{T}}{\partial x_j} = \frac{\nu_t}{\mathrm{Pr}_t}\frac{\partial\overline{T}}{\partial x_j} \tag{10}$$

$$-\overline{v_j'C'} = D_t\frac{\partial\overline{C}}{\partial x_j} = \frac{\nu_t}{\mathrm{Sc}_t}\frac{\partial\overline{C}}{\partial x_j} \tag{11}$$

where $k_t$ and $D_t$ are the turbulent diffusivity coefficients for the heat and pollutant transport equations. These SGS terms are obtained using the eddy diffusivity assumption, where the turbulent Prandlt number $\mathrm{Pr_t}$ and the turbulent Schmidt number $\mathrm{Sc_t}$ are utilized.

The final form of the filtered governing equations, considering the eddy viscosity approach for the SGS terms, may be presented as follows:

$$\frac{\partial\overline{v}_i}{\partial t} + \overline{v}_j\frac{\partial\overline{v}_i}{\partial x_j} = -\frac{1}{\rho}\frac{\partial\overline{p}}{\partial x_i} + \frac{\partial}{\partial x_j}\left[2\left(\nu+\nu_t\right)\overline{S}_{ij} + \frac{\lambda}{\rho}\frac{\partial\overline{v}_k}{\partial x_k}\right] + \frac{1}{\rho}\overline{S}_i \qquad (\mathrm{i,j,k}=1,2,3) \qquad \text{in } \Omega \tag{12}$$

$$\frac{\partial\overline{p}}{\partial t} + \overline{v}_j\frac{\partial\overline{p}}{\partial x_j} + \rho c_s^2\frac{\partial\overline{v}_j}{\partial x_j} = 0 \qquad (\mathrm{j}=1,2,3) \qquad \text{in } \Omega \tag{13}$$

$$\frac{\partial\overline{T}}{\partial t} + \overline{v}_j\frac{\partial\overline{T}}{\partial x_j} = \frac{\partial}{\partial x_j}\left[\left(\frac{k}{\rho c_v} + \frac{\nu_t}{\mathrm{Pr}_t}\right)\frac{\partial\overline{T}}{\partial x_j}\right] + \frac{1}{c_v}\overline{S}_T \qquad (\mathrm{j}=1,2,3) \qquad \text{in } \Omega \tag{14}$$

$$\frac{\partial\overline{C}}{\partial t} + \overline{v}_j\frac{\partial\overline{C}}{\partial x_j} = \frac{\partial}{\partial x_j}\left[\left(D + \frac{\nu_t}{\mathrm{Sc}_t}\right)\frac{\partial\overline{C}}{\partial x_j}\right] + \overline{S}_P \qquad (\mathrm{j}=1,2,3) \qquad \text{in } \Omega \tag{15}$$

Smagorinsky (1963) proposed to relate the eddy viscosity to the large scale flow field and the size of the numerical grid by using the following expression:

$$\nu_t = \left(C_S\overline{\Delta}\right)^2\left|\overline{\mathbf{S}}\right| \tag{16}$$

where $\overline{\Delta}$ is the characteristic filter width, which may be locally obtained from the element volume for FEM formulations ($\overline{\Delta} = \sqrt[3]{\overline{\Delta}_1\cdot\overline{\Delta}_2\cdot\overline{\Delta}_3}$), $\left|\overline{\mathbf{S}}\right|$ is the modulus of the strain rate tensor and $C_S$ is an empiric constant known as Smagorinsk's constant, with values usually ranging from 0.1 to 0.25. However, it is observed that $C_S$ is not a universal constant, but it is flow dependent. In order to eliminate this shortcoming, the eddy viscosity $\nu_t$ can be also obtained employing the dynamic SGS model developed by Germano et al. (1991) and Lilly (1992), which may be expressed as:

$$\nu_\mathrm{t} = C\left(\vec{x},t\right)\overline{\Delta}^2\left|\overline{\mathbf{S}}\right| \tag{17}$$

where $C(\vec{x},t)$ is the dynamic coefficient, with $\vec{x}$ and $t$ indicating space and time dependencies. The dynamic coefficient is updated along the time integration process taking into account instantaneous conditions of the flow field, that is:

$$C(\vec{x},t) = -\frac{1}{2}\frac{L_{ij}M_{ij}}{M_{ij}M_{ij}} \tag{18}$$

where:

$$L_{ij} = \left\langle \overline{v}_i \overline{v}_j \right\rangle - \left\langle \overline{v}_i \right\rangle \left\langle \overline{v}_j \right\rangle \tag{19}$$

and:

$$M_{ij} = \left\langle \overline{\Delta} \right\rangle^2 \left| \left\langle \overline{S} \right\rangle \right| \left\langle \overline{S}_{ij} \right\rangle - \left\langle \overline{\Delta}^2 \left| \overline{S} \right| \overline{S}_{ij} \right\rangle \tag{20}$$

Nevertheless, the solution of Eq. (18) requires two filtering procedures on the flow governing equations: the first filtering is associated with the use of the LES formulation, where the spatial filter $\overline{\Delta}$ is applied in order to define the large scale variables $\overline{\phi}$; the second filtering is referred to another filter called test filter $\left\langle \overline{\Delta} \right\rangle$, which must be larger than the width of the first spatial filter $\overline{\Delta}$. Additional information on the evaluation of the filtered variables related to the second spatial filter is found in Braun and Awruch (2009b).

### 2.3 Numerical model

The numerical algorithm for the flow analysis is formulated considering the two-step Taylor-Galerkin model (see Braun and Awruch, 2009a). In this method, the governing equations are temporally discretized using second-order Taylor series expansions and the Bubnov-Galerkin method is applied to the system of equations obtained from the time discretization procedure. Finite element approximations for the spatial and variable fields are performed here considering the eight-node hexahedral element formulation. The element matrices are evaluated employing the one-point quadrature technique, where the origin of the parametric space is chosen as the only quadrature point. This integration technique leads to analytical evaluation of the matrix components, which is exact for elements with parallel faces. Good results can be also obtained for slightly distorted elements, but they are not strictly exact. Nevertheless, spurious modes (hourglass modes) must be suppressed using some hourglass control scheme in order to obtain reliable results. An algorithm describing the numerical scheme utilized here to solve the governing equations may be found in Table 1, where the overbars representing the large scale variables are omitted for the sake of simplicity.

1) *The first step*: calculate the flow variables at the intermediate point of the time increment $\Delta t$:

$$v_i^{n+1/2} = v_i^n + \frac{\Delta t}{2}\left\{ -v_j\frac{\partial v_i}{\partial x_j} - \frac{1}{\rho}\frac{\partial p}{\partial x_j}\delta_{ij} + \frac{\partial}{\partial x_j}\left[ (\nu + \nu_t)\left( \frac{\partial v_i}{\partial x_j} + \frac{\partial v_j}{\partial x_i} \right) + \frac{\lambda}{\rho}\frac{\partial v_k}{\partial x_k}\delta_{ij} \right] + \left( \frac{\Delta t}{4} v_j v_k \right)\frac{\partial^2 v_i}{\partial x_j x_k} + \frac{S_i}{\rho} \right\}^n$$

$$p^{n+1/2} = p^n + \frac{\Delta t}{2}\left\{ \left[ -v_j\frac{\partial p}{\partial x_j} - \rho c^2\frac{\partial v_j}{\partial x_j} \right] + \left( \frac{\Delta t}{4} v_i v_j \right)\frac{\partial^2 p}{\partial x_j \partial x_i} \right\}^n$$

$$T^{n+1/2} = T^n + \frac{\Delta t}{2}\left\{-v_j\frac{\partial T}{\partial x_j} + \left(\frac{k}{\rho c_v} + \frac{\nu_t}{\mathrm{Pr}_t}\right)\frac{\partial^2 T}{\partial x_j^2} + \left(\frac{\Delta t}{4}v_i v_j\right)\frac{\partial^2 T}{\partial x_j \partial x_i} + \frac{1}{c_v}S_T\right\}^n$$

$$C^{n+1/2} = C^n + \frac{\Delta t}{2}\left\{-v_j\frac{\partial C}{\partial x_j} + \left(D + \frac{\nu_t}{\mathrm{Sc}_t}\right)\frac{\partial^2 C}{\partial x_j^2} + \left(\frac{\Delta t}{4}v_i v_j\right)\frac{\partial^2 C}{\partial x_j \partial x_i} + S_C\right\}^n$$

2) Apply the boundary conditions on $v_i^{n+1/2}$, $p^{n+1/2}$, $T^{n+1/2}$ and $C^{n+1/2}$.

3) Calculate the pressure increment $\Delta p^{n+1/2} = p^{n+1/2} - p^n$.

4) Calculate the corrected velocity field with the updated pressure $\Delta p^{n+1/2}$:

$$v_i^{n+1/2} = v_i^{n+1/2} - \frac{1}{\rho}\frac{\Delta t^2}{8}\frac{\partial \Delta p^{n+1/2}}{\partial x_i}$$

5) Apply the boundary condition on $v_i^{n+1/2}$.

6) *The second step*: update the flow variables at the end of the time increment $\Delta t$:

$$v_i^{n+1} = v_i^n + \Delta v_i^{n+1/2}$$

$$p^{n+1} = p^n + \Delta p^{n+1/2}$$

$$T^{n+1} = T^n + \Delta T^{n+1/2}$$

$$C^{n+1} = C^n + \Delta C^{n+1/2}$$

where:

$$\Delta v_i^{n+1/2} = \Delta t\left\{-v_j\frac{\partial v_i}{\partial x_j} - \frac{1}{\rho}\frac{\partial p}{\partial x_j}\delta_{ij} + \frac{\partial}{\partial x_j}\left[(\nu + \nu_t)\left(\frac{\partial v_i}{\partial x_j} + \frac{\partial v_j}{\partial x_i}\right) + \frac{\lambda}{\rho}\frac{\partial v_k}{\partial x_k}\delta_{ij}\right] + \frac{S_i}{\rho}\right\}^{n+1/2}$$

$$\Delta p^{n+1/2} = \Delta t\left\{-v_j\frac{\partial p}{\partial x_j} - \rho c^2\left(\frac{\partial v_j}{\partial x_j}\right)\right\}^{n+1/2}$$

$$\Delta T^{n+1/2} = \Delta t\left\{-v_j\frac{\partial T}{\partial x_j} + \left(\frac{k}{\rho c_v} + \frac{\nu_t}{\mathrm{Pr}_t}\right)\frac{\partial^2 T}{\partial x_j^2} + \frac{1}{c_v}S_T\right\}^{n+1/2}$$

$$\Delta C^{n+1/2} = \Delta t\left\{-v_j\frac{\partial C}{\partial x_j} + \left(D + \frac{\nu_t}{\mathrm{Sc}_t}\right)\frac{\partial^2 C}{\partial x_j^2} + \frac{1}{c_p}S_C\right\}^{n+1/2}$$

7) Apply the boundary conditions on $v_i^{n+1}$, $p^{n+1}$, $T^{n+1}$ and $C^{n+1}$.

8) Return to 1) for the next time step $\Delta t$.

Table 1. Numerical algorithm for the flow analysis.

The time interval used in the time discretization scheme is restricted by the Courant condition in order to maintain numerical stability, since the time integration is carried out explicitly. A critical value can be calculated at element level by using the following expression:

$$\Delta t_{\mathrm{E}} = \alpha\frac{\Delta x_{\mathrm{E}}}{\mathrm{V}_{\mathrm{E}} + c_s} \qquad \mathrm{E} \in [1, NE] \tag{21}$$

where $\Delta x_E$ is the characteristic width of element $E$, $\mathrm{V}_E$ is a characteristic flow speed of element $E$, $c_s$ is the sound speed in the flow field, $\alpha$ is a safety constant, which is generally less than unity, and $NE$ is the number of elements in the finite element mesh. Although

independent time steps can be adopted, the time step employed in the numerical applications carried out in this work is obtained from the smaller time step calculated with Eq. (21).

Moreover, in order to improve the computational efficiency of the numerical code developed in this work, all do loops were parallelized using OpenMP Application Program Interface. Two intel(R) Xeon(R) E5 2690 processors (16 cores in total) with 64 Gb RAM was utilized in the tests presented here.

## 3 MODEL VALIDATION

In order to validate the model presented in this work, flow and pollutant dispersion in two problems were analyzed: (a) a two-dimensional street canyon model with AR = H/W = 1.0, under isothermal conditions, which was studied experimentally by Meroney et al. (1996) and Pavageau and Schatzmann (1999); (b) a two-dimensional lid-driven cavity, under isothermal and non-isothermal conditions, which was studied numerically by Ghia et al (1982) and Agrawal et al. (2001). It will be shown later that results obtained in both cases present good agreement with those obtained by the authors mentioned previously.

Geometric characteristics, boundary conditions and the finite element mesh utilized here are shown in Fig.1 (a) and Fig. 1 (b). No-slip boundary conditions are imposed on solid surfaces and the flow variables are started with zero as initial conditions for both problems. In the case of the lid-driven cavity a vertical gradient is imposed on the temperature field if non-isothermal conditions are analyzed. The time step is chosen taking into account Eq. (21).

For the street canyon model, the spatial field is discretized using 8400 elements where the smaller elements are found along the canyon walls, with $\Delta x_E = 0.001$ m. A pollutant is emitted from a point source located at the bottom of the canyon model (see Fig. 1 (a)) and the emission rate is defined as $S_P = 2.89 \times 10^{-5}$ m$^3$/s. The dimensionless numbers adopted were: $Re = 1.2 \times 10^4$ and $Sc = Sc_t = 0.72$. The Reynolds number is evaluated considering the height (H) of the street canyon model and the undisturbed flow velocity at z = 0.65 m, i.e. $V\infty = 2.0$ m/s (see Fig. 1 (a)). The safety factor and the time step are $\alpha = 0.27$ and $\Delta t = 10^{-5}$ s, respectively. Turbulence is simulated using LES with the dynamic SGS model.

Numerical analyses were performed up to t = 110 s, where a time average flow field with statistically constant characteristics is obtained. The time average fields were calculated taking into account the last 10 s of the present analyses.

For the lid-driven cavity analysis, 100x100 elements are utilized with the most refined elements located along the cavity walls ($\Delta x_E = 0.0025$ m). The dimensionless numbers adopted are presented in the Fig. 3, where $Pr = Pr_t = 0.71$ when non-isothermal conditions are considered. The safety factor and the time step are $\alpha = 0.44$ and $\Delta t = 10^{-4}$ s, respectively. Turbulence is simulated using LES with Smagorinsky`s SGS model considering $C_S = 0.15$.

It is important to mention that although 3-D hexahedral elements were used, when 2-D applications are considered, only one element was employed in the normal direction to the plane where the domain is contained. The velocity component, normal to the problem domain, was canceled in all finite element nodes in order to establish the condition of symmetry in this direction for the flow, heat and mass transfer.

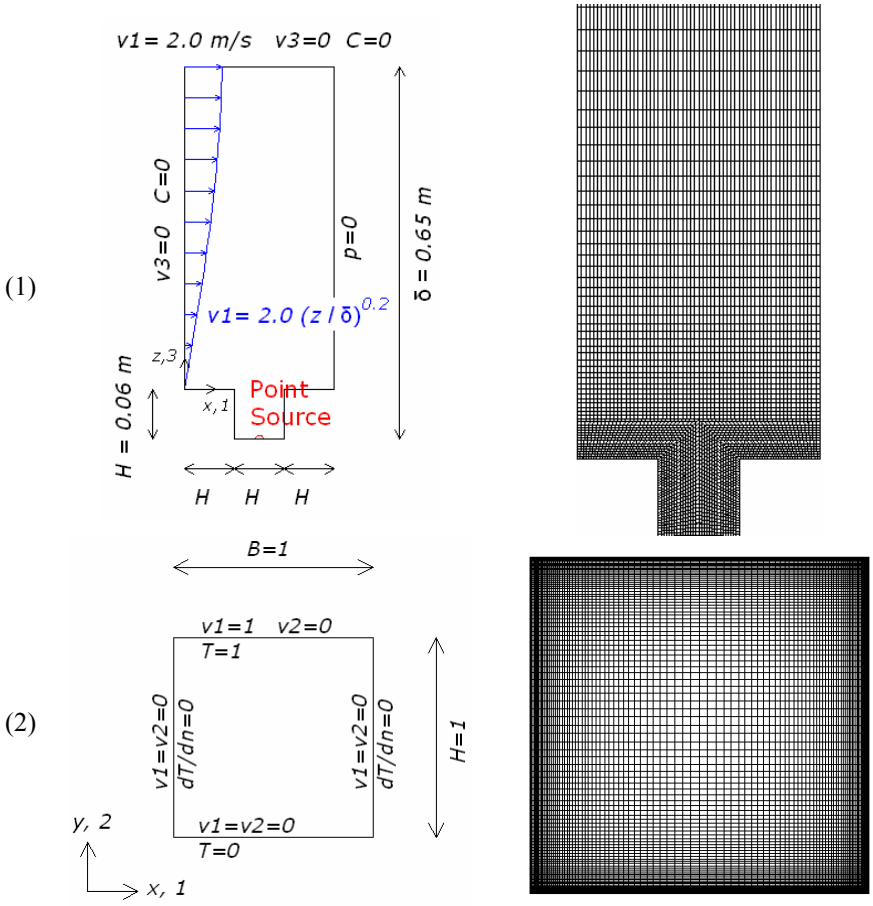


Figure 1. Model validation: (1) 2-D street canyon; (2) 2-D lid-driven cavity; (a) geometrical domain and boundary conditions; (b) finite element mesh.

Fig. 2 shows the results obtained with the numerical model proposed in this work for the street canyon analysis. Profiles referring to the dimensionless pollutant concentration K measured along vertical and horizontal lines of the canyon model are also presented in Fig. 2 (f) and Fig. 2 (g), respectively and they are compared with results obtained experimentally by Meroney et al. (1996) and Pavageau and Schatzmann (1999), considering that the reference length utilized in the definition of the Reynolds number, $H_{ref}$, are equal to 1.0H and 3.0H, respectively. One can observe that a good agreement is obtained considering comparisons performed with respect to concentration distribution in the canyon cavity, especially when $H_{ref}$ = 3.0H is adopted.

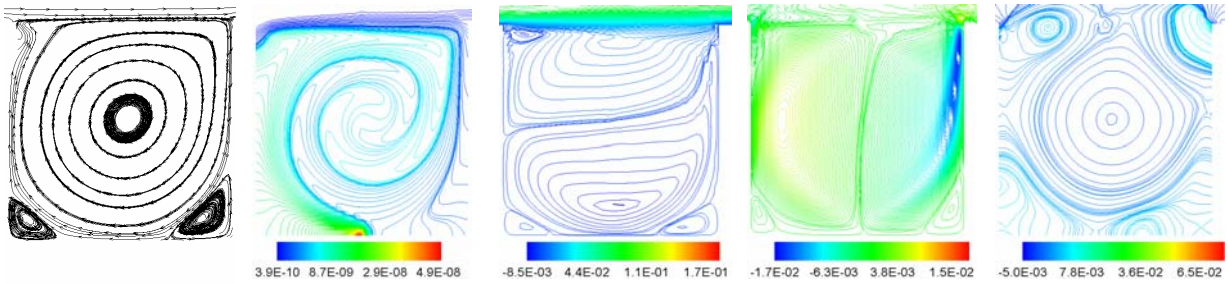

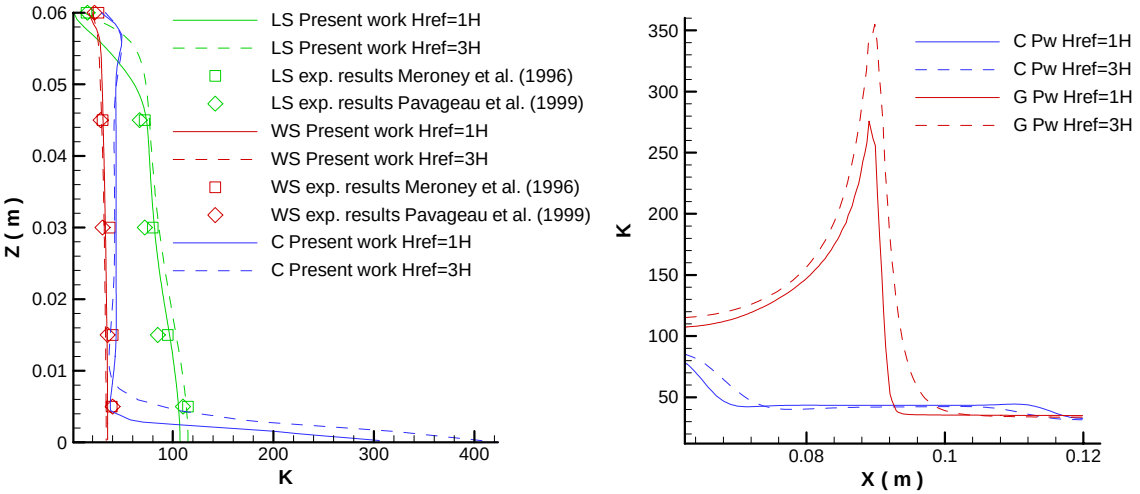


(f) (g)

Figure 2. Two-dimensional street canyon: time average fields in the canyon – (a) streamlines; (b) pollutant concentration; (c)flow velocity components v1; (d) flow velocity components v3; (e) pressure; (f) dimensionless concentration K distributions along vertical lines - on the leeward side (LS), windward side (WS) and central line (C); (g) horizontal lines – on the central line (C) and near ground level (G).

Fig. 3 shows results obtained in the lid-driven cavity investigation. Velocity profiles obtained with the present model along the horizontal and vertical centerlines of the cavity for all the flow conditions investigated are also shown in Fig. 3, where they are satisfactorily compared with numerical predictions obtained by Ghia et al. (1982) and Agrawal et al. (2001).

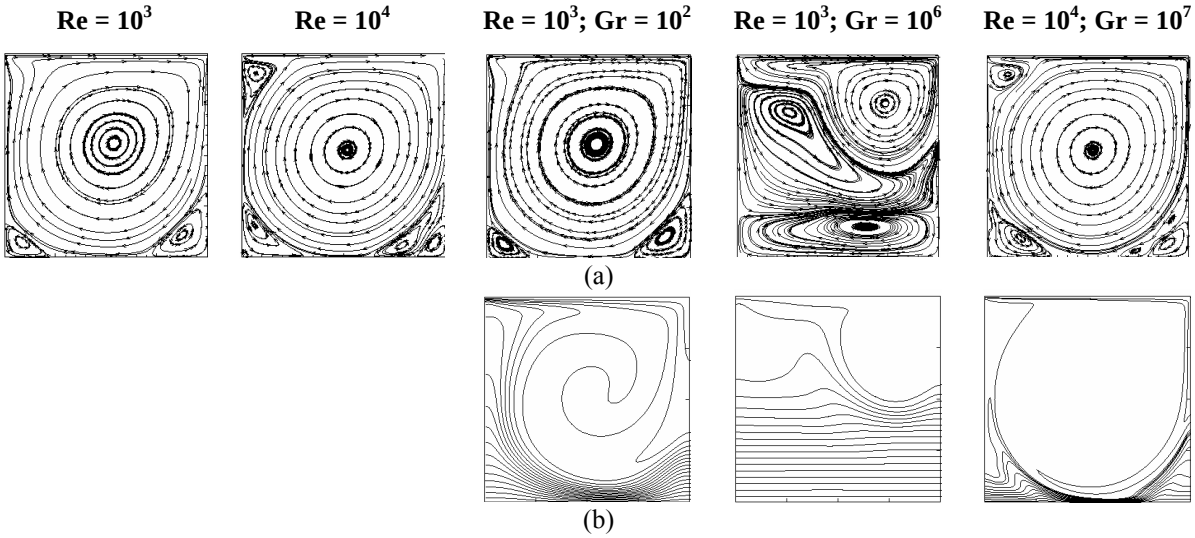

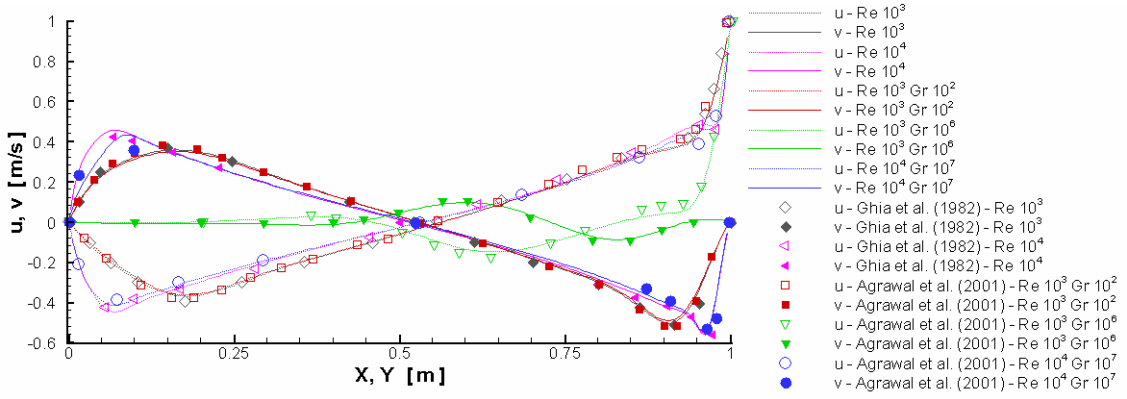


(c)

Figure 3. Lid-driven cavity analysis: (a) streamlines; (b) isotherms; (c) velocity profiles along the centerlines of the cavity for different flow conditions.

## 4 NUMERICAL APPLICATIONS

### 4.1 Pollutant dispersion in an urban area

A real application considering the evaluation of wind conditions and pollutant dispersion around a cluster of buildings is proposed in the present analysis, which is based on the studies carried out by Stathopoulos and Baskaran (1996), who investigated the wind environmental conditions around a block of buildings using experimental and numerical techniques. A model representing a region of downtown Montreal was selected for this purpose, where the building models were assumed to have rectangular shape and details of the external surface were omitted. Since the investigations performed by Stathopoulos and Baskaran (1996) were carried out considering incompressible flows without heat or mass transfer, low linear sources of a pollutant are proposed in order to analyze the pollutant dispersion in this case. A schematic view of the computational domain utilized here and the mesh configuration in the region of the buildings are found in Fig. 4, where geometric information on the building models and boundary conditions are indicated. The finite element mesh is constituted by 1268272 eight-node hexahedral elements, with $\Delta x_E \approx 0.2$ m, which is related to the smaller elements located along the building and ground surfaces. The positions of the linear pollutant sources, which approximately reproduce emission conditions observed under intense traffic of motor vehicles, are also shown. The pollutant sources are characterized with an emission rate of $S_P = 0.01$ m$^3$/s.

In order to verify the differences observed between two and three-dimensional modeling, a two-dimensional simulation was also carried out considering the central plane xz (y = 331.25 m) of the three-dimensional computational space utilized previously, where the time average results obtained with the two and three-dimensional models were compared. The two-dimensional analysis was carried out considering the same geometric configuration, the same mesh refinement and the same boundary conditions (except for the velocity component $v_2$, which is admitted to be equal to zero throughout the domain when the two-dimensional model is adopted) employed in the central plane of the computational model referring to the three-dimensional analysis.

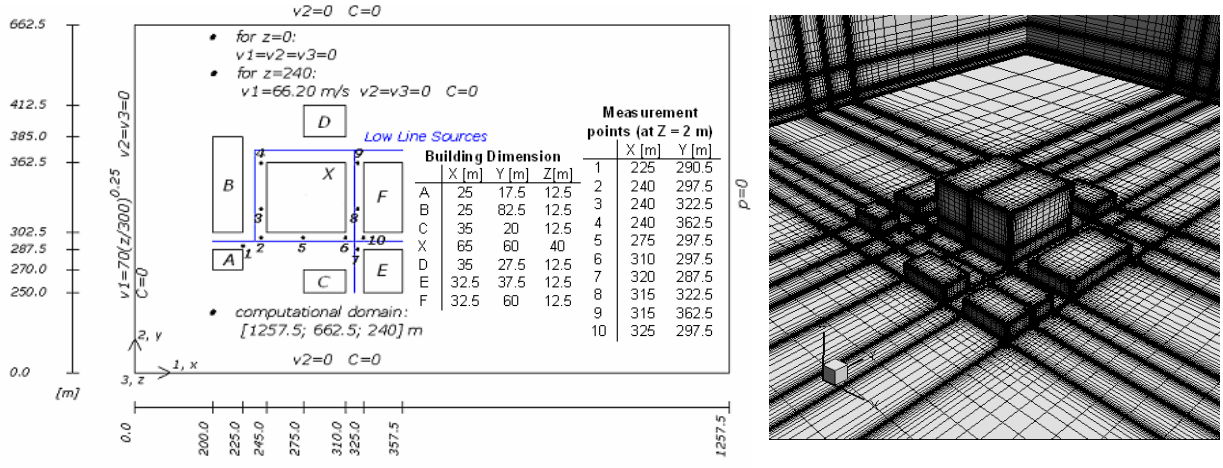


Figure 4. Three-dimensional urban area analysis: (a) computational domain; (b) finite element mesh.

The flow properties are characterized by the following dimensionless numbers: Re = 1.69 x $10^8$, Sc and $Sc_t$ = 0.72, where an isothermal process is assumed. Turbulence is simulated considering LES and the classical Smagorisky's SGS model, where $C_S$ = 0.10. The flow variables are started with zero initial conditions, where the time step is chosen taking into account Eq. (21) with $\alpha$ = 0.80, which leads to $\Delta t = 6.0 \times 10^{-4}$ s. The Reynolds number is obtained considering the width of building X and the flow velocity at the roof level of the same building (see Fig. 4). The numerical analysis was carried out up to t = 150 s and time average fields were obtained over the last 40 s of the present simulation.

In Fig. 5 some comparisons are made between results obtained with the present model and numerical and experimental predictions obtained by Stathopoulos and Baskaran (1996) for the urban model investigated here. Measurements were performed considering the points indicated in Fig. 4 and the corresponding flow parameters, such as the velocity ratio $V_1/V_0$, where $V_1 = \sqrt{v_1^2 + v_2^2}$ and $V_0$ is the undisturbed streamwise flow velocity component defined at z = 2 m. It is observed that the present numerical results show a better agreement with experimental data than the numerical results obtained by Stathopoulos and Baskaran (1996).

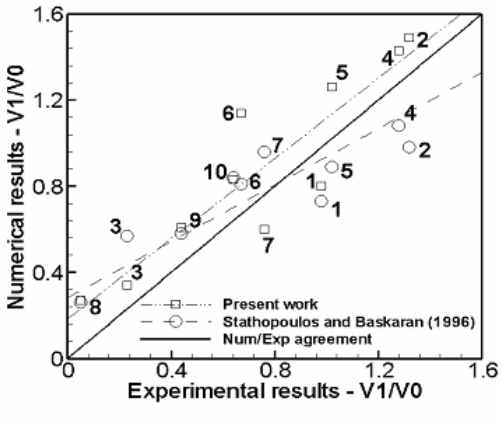


Figure 5.Three-dimensional urban area analysis: comparison between experimental and numerical results obtained in the present work

Time average streamlines obtained in the 3d analysis are shown in Fig. 6, where important

flow phenomena such as horseshoe vortices can be observed (see Fig. 6 (b)). Two street canyons are formed upstream and downstream the highest building of the block configuration, where, for the upstream canyon, a recirculation zone which leads to the removal of the fluid and pollutants by the lateral ends of the canyon can be noticed (see Fig. 6 (f)). This recirculation zone has significant influence over the pollutant concentration in the street canyon and it is not observed when 2-D models are considered, as one can see in the following analysis.

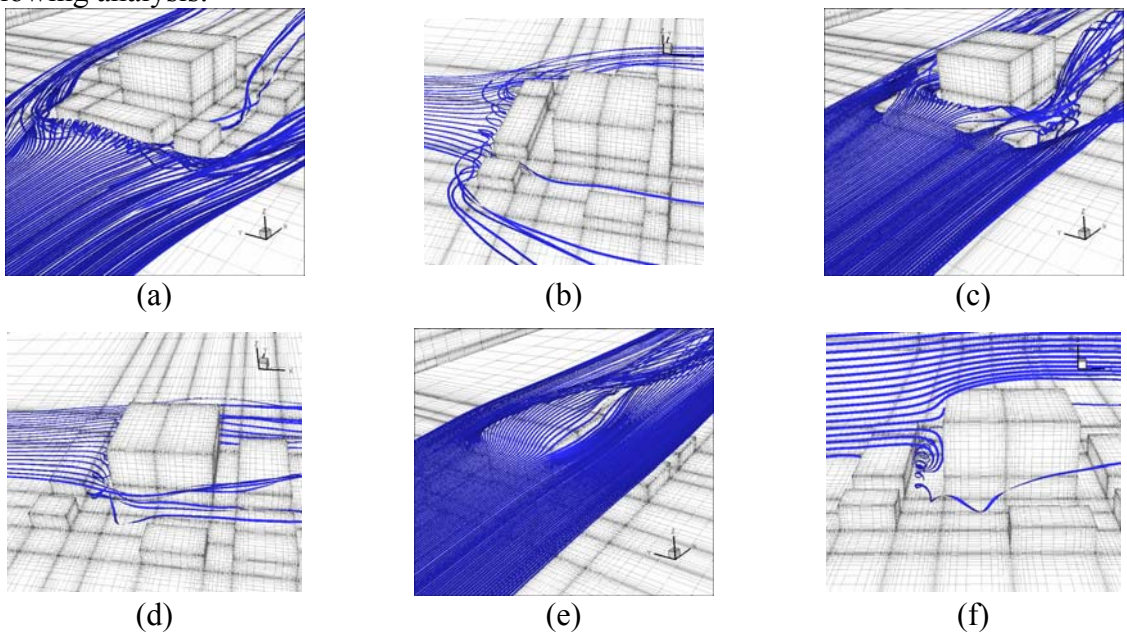


Figure 6. Three-dimensional urban area analysis: time average streamlines (a) at z = 1 m; (b) at z = 2.0 m; (c) at z = 5 m; (d) at z = 11.0 m; (e) at z = 25 m; (f) at y = 332.5 m.

Fig. 7 presents the streamlines, pressure and pollutant concentration fields corresponding to the central plane of the spatial domain, where predictions obtained with the two-dimensional and three-dimensional analyses are compared. In both analysis, the recirculation region developed upstream building X reaches a steady state while the downstream recirculation maintains a transient condition.

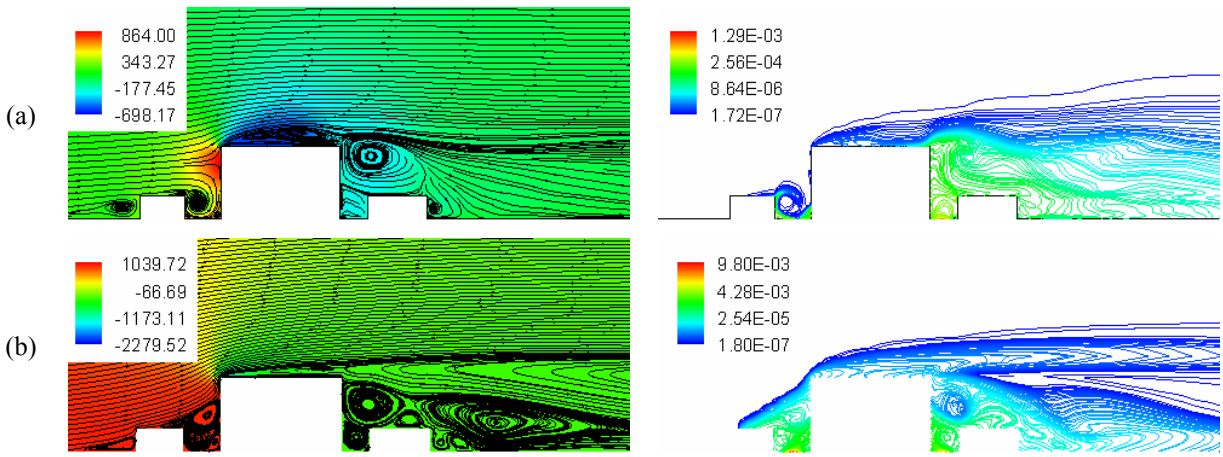


Figure 7. Urban area analysis – time average fields on plane y = 332.5 m: pressure and streamlines (first column) and pollutant concentration field (second column) considering (a) 3d analysis and (b) 2d analysis.

Streamlines, velocity components $v_1$, $v_2$ and $v_3$ and pollutant concentration fields obtained

in the vicinity of canyon BX (which is the canyon formed between B and X buildings) and in the vicinity of canyon XF (which is the canyon formed between X and F buildings), considering two and three-dimensional analyses, are shown in Fig. 8 and Fig. 9, respectively.

Inside canyon BX, considering the three-dimensional analysis, one can observe the formation of a primary clockwise recirculation and two small vortices in the lower corners. On the other hand, two primary recirculation in opposite directions and small vortices in the lower corners are formed when the predictions obtained with the two-dimensional model are observed. Assimakopoulos et al. (2003) studied similar configurations (the upstream building is shorter than the downstream building) employing a two-dimensional RANS model and found a single primary clockwise circulation region in the canyon cavity, which can be related to the higher dissipation effect presented in RANS models. The velocity fields obtained here are different, since the velocity component $v_2$, which was not considered in the two-dimensional analysis, is present in the three-dimensional analysis and modifies the $v_1$ and $v_3$ velocity fields, altering the pollutant concentration distribution consequently. One can see that the pollutant concentration inside canyon BX is higher when the two-dimensional model is utilized. The incidence of three-dimensional vortices with streamlines moving towards the end of the canyon (see Fig 6 (f)) contributes to the pollutant removal, leading to a lower pollutant concentration when the three-dimensional analysis is carried out. Due to the two primary recirculation regions observed in the prediction referring to the two-dimensional analysis, which are rotating in opposite directions, one can see that there is a higher pollutant retention inside the canyon and the pollutant concentration reaches higher levels along the canyon walls.

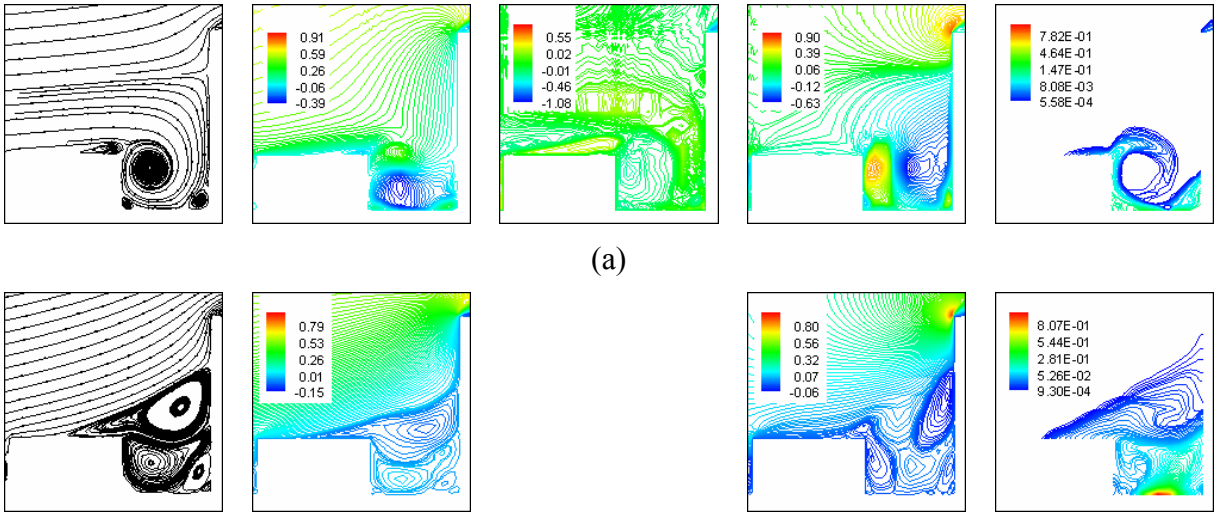


Figure 8. Urban area analysis – streamlines; normalized velocity components $v_1$, $v_2$ and $v_3$ and time average fields of normalized pollutant concentration on plane y = 332.5 m in the vicinity of canyon BX: (a) 3d analysis and (b) 2d analysis.

Downstream building X one can see a primary recirculation region carrying the pollutant from canyon XF (canyon formed between buildings X and F) to the roof of the building X, which is observed in the both analyses performed here (see Fig. 7). This recirculation region presents clockwise rotation and counterclockwise rotation when the three and two-dimensional models are utilized, respectively. Assimakopoulos et al. (2003) studied similar configurations (the upstream building is higher than the downstream building) employing a two-dimensional RANS model and reported a clockwise circulation zone in this region.

One can observe that a primary clockwise recirculation zone and a small vortex in the lower corner are formed inside canyon XF when the two-dimensional analysis is carried out, leading to velocity and pollutant concentration fields similar to those fields observed in street canyons with unit aspect ratio. On the other hand, in the three-dimensional analysis, velocity component $v_2$ is present, which alters the $v_1$ and $v_3$ velocity fields, carrying the pollutant towards y direction and leading to lower levels of pollutant concentration. The $v_1$ and $v_3$ velocity components present values near to zero and the pollutant transport occurs mainly due to diffusive processes.

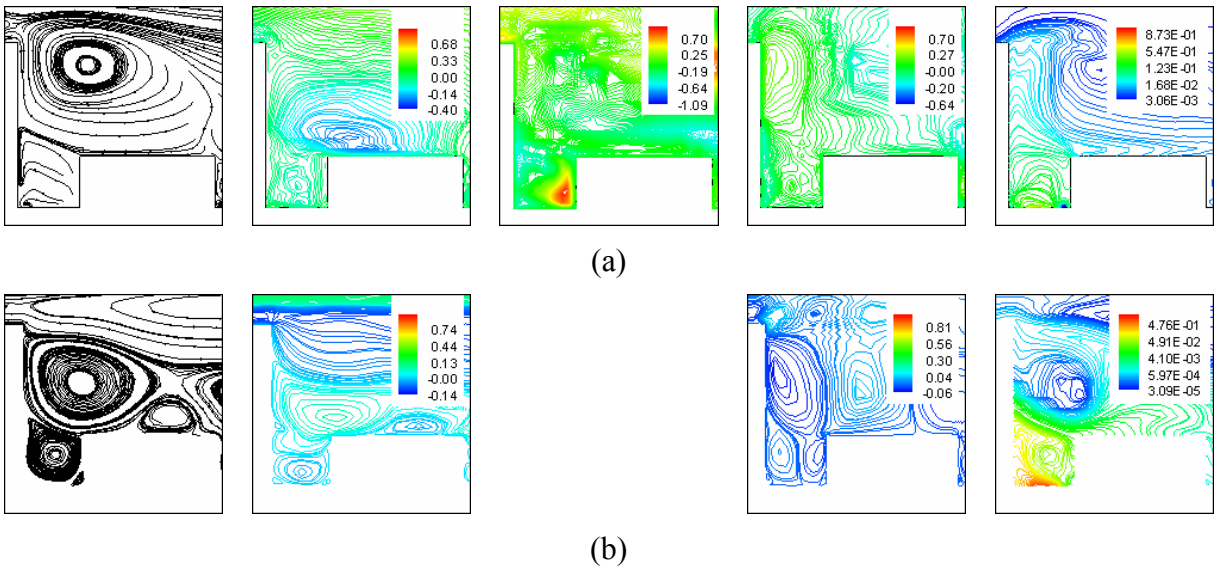


Figure 9. Urban area analysis – streamlines; normalized velocity components $v_1$, $v_2$ and $v_3$ and time average fields of normalized pollutant concentration on plane y = 332.5 m and in the vicinity of canyon XF: (a) 3d analysis and (b) 2d analysis.

As mentioned before, due to the existence of the $v_2$ velocity component, different flow behaviors can be observed when the predictions obtained with the two-dimensional and three-dimensional models are compared. Due to the same reason, different results for the flow variables were also observed. In Table 2, the maximum values for pollutant concentration and flow velocity components are presented considering the analyses performed here.

| | $C_{max}$ | $V_{1max}$ | $V_{2max}$ | $V_{3max}$ |
|---|---|---|---|---|
| **2d analysis** | 0.010 | 78.069 | 0.000 | 50.825 |
| **3d analysis** | 0.001 | 66.324 | 7.834 | 45.594 |

Table 2. Urban area analysis – maximum values obtained for pollutant concentration and flow velocity components.

### 4.2 Pollutant dispersion in an urban street canyon

In order to compare predictions obtained with LES and different SGS modeling, a street canyon configuration presenting two parallel buildings with aspect ratio H/W=1 is investigated considering analyses performed with two and three-dimensional models. The present application was previously analyzed by Gromke and Ruck (2007; 2009; 2012) where experimental procedures were employed, and Salim et al. (2011), where numerical simulations were carried out.

A schematic view of the computational domain utilized here and the mesh configuration in the region of the buildings are found in Fig. 10, where boundary conditions are also indicated. The finite element mesh is constituted by 1326950 eight-node hexahedral elements, with $\Delta x_E \approx 0.05$ m, which is related to the smaller elements located along the building and ground surfaces. The positions of the linear pollutant sources, which approximately reproduce emission conditions observed under intense traffic of motor vehicles, are also shown. In order to account for the traffic exhausts released on sidewise street intersections, the line sources exceed the street canyon length by approximately 10% on each side. The pollutant sources are characterized with an emission rate of $S_P = 0.01$ m$^3$/s. A two-dimensional analysis was also carried out considering the same mesh refinement employed in the central plane (y=60m) of the three-dimensional model.

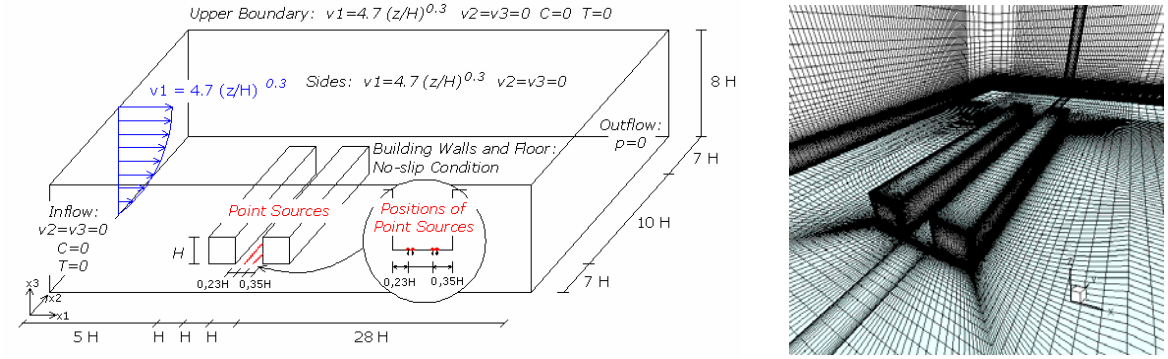


(a) (b)

Figure 10. Three-dimensional street canyon: (a) geometrical domain and boundary conditions; (b) finite element mesh.

The flow properties adopted in the numerical model are characterized by the following dimensionless numbers: Re = 3.76 x $10^4$, Ma = 0.16 and Sc = $Sc_t$ = 0.7. Turbulence is simulated considering LES and both, the classical Smagorisky's SGS model ($C_S$ = 0.12) and the dynamic SGS model. The flow variables are started with zero initial conditions, where the time step is chosen taking into account Eq. (21) with $\alpha = 0.51$, which leads to $\Delta t = 7.5 \times 10^{-4}$ s. The Reynolds number is obtained considering the building height and the flow velocity at the roof level (see Fig. 10 (a)). The numerical analysis was carried out up to t = 2000 s and time average fields were obtained over the last 200 s of the present simulation.

Fig. 11 presents the time average streamlines and time average pressure fields for the plane x - z (y = 60 m), obtained when the classical Smagorisky's SGS model [CM] and the dynamic SGS model [DM] were used. For both turbulence models employed here, one can notice that the streamlines passing through the first building detach and don't reattach along the top surface of this building, forming a small recirculation zone above the roof of the first building. A main clockwise recirculation zone and two secondary counterclockwise vortices located at the corners of the canyon are formed in the canyon cavity. Behind the second building, a stationary secondary counterclockwise vortex is formed near the floor, which streamlines do not communicate with the internal flow of the canyon. A recirculation zone, which extends over a distance of 3H in the flow direction, is generated near the rear wall and above the stationary vortex mentioned previously. The clockwise recirculation generated inside the canyon extends in the vertical direction beyond the height of the buildings and in the horizontal direction over the top of the upstream building. However, when the dynamic model is employed, the recirculation generated inside the canyon also extends in the horizontal direction over the top of the downstream building.

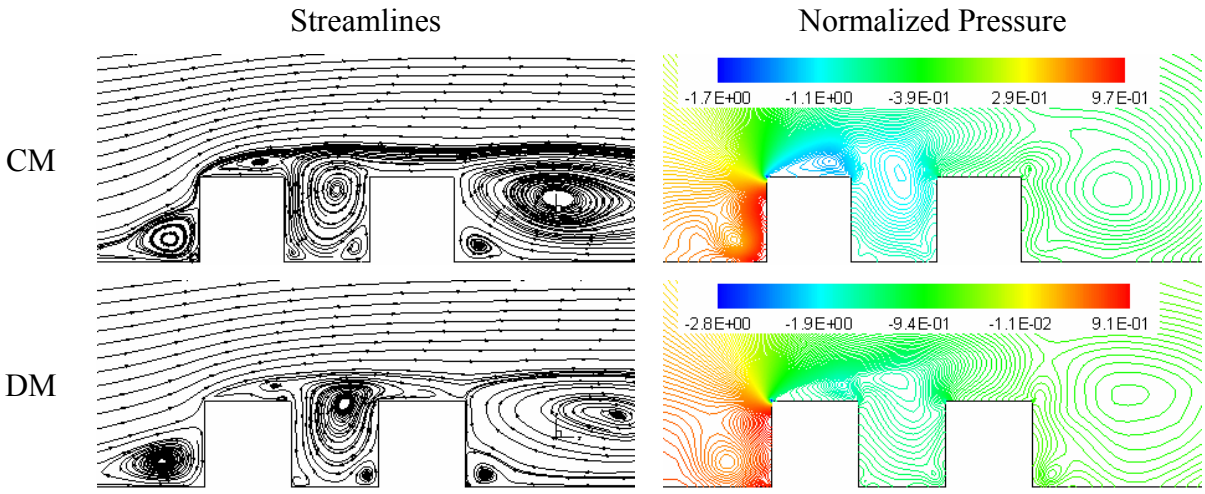


Figure 11. Three-dimensional street canyon: time average fields on plane y = 60 m – streamlines and normalized pressure field.

In Fig. 12 one can see the time average streamlines and fields for normalized pollutant concentration and velocity components related to the plane x – z (y = 60 m). Analyzing these figures, one can notice that, for both turbulence models used in this work, the secondary vortices, which are located inside the canyon, spread the pollutant in the region near the ground. According to the direction of the main recirculation developed inside the canyon, the pollutants are removed from the canyon. Since there is a clockwise main recirculation zone located in this region, the pollutants tend to be removed through the leeward wall (wall A). Through the flow developed in the upper region of the canyon, the pollutants carried by the main flow in the opposite direction to the top of the first building and then, they are carried downstream by the main flow.

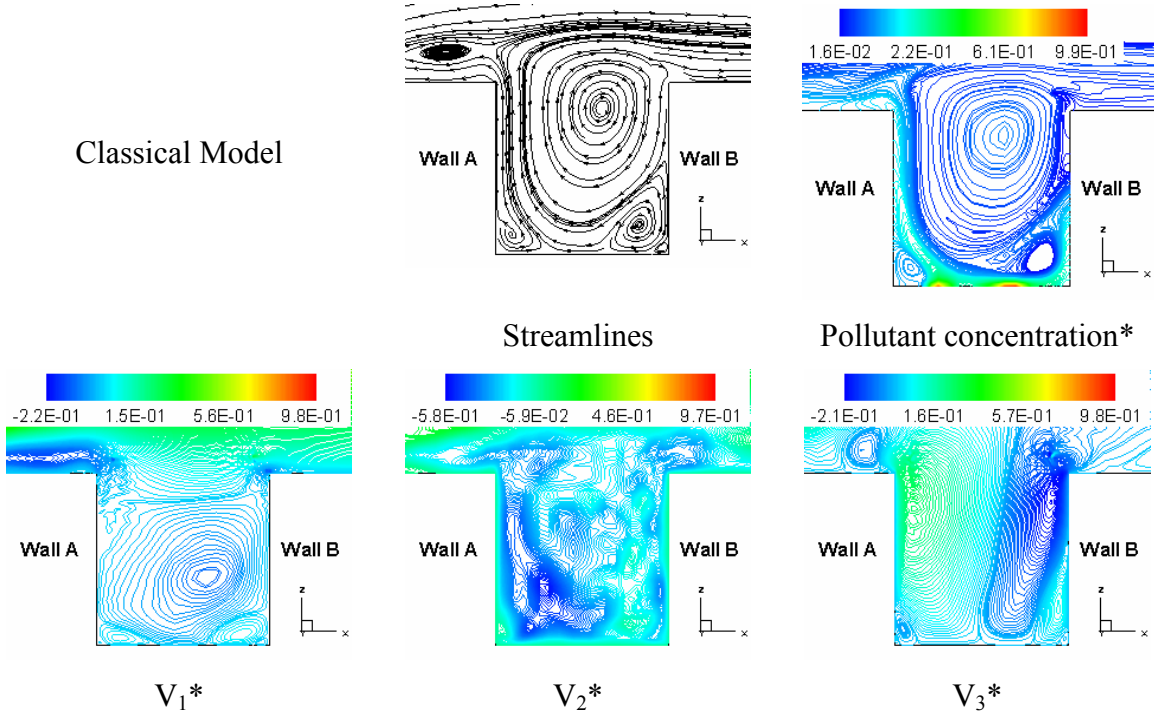

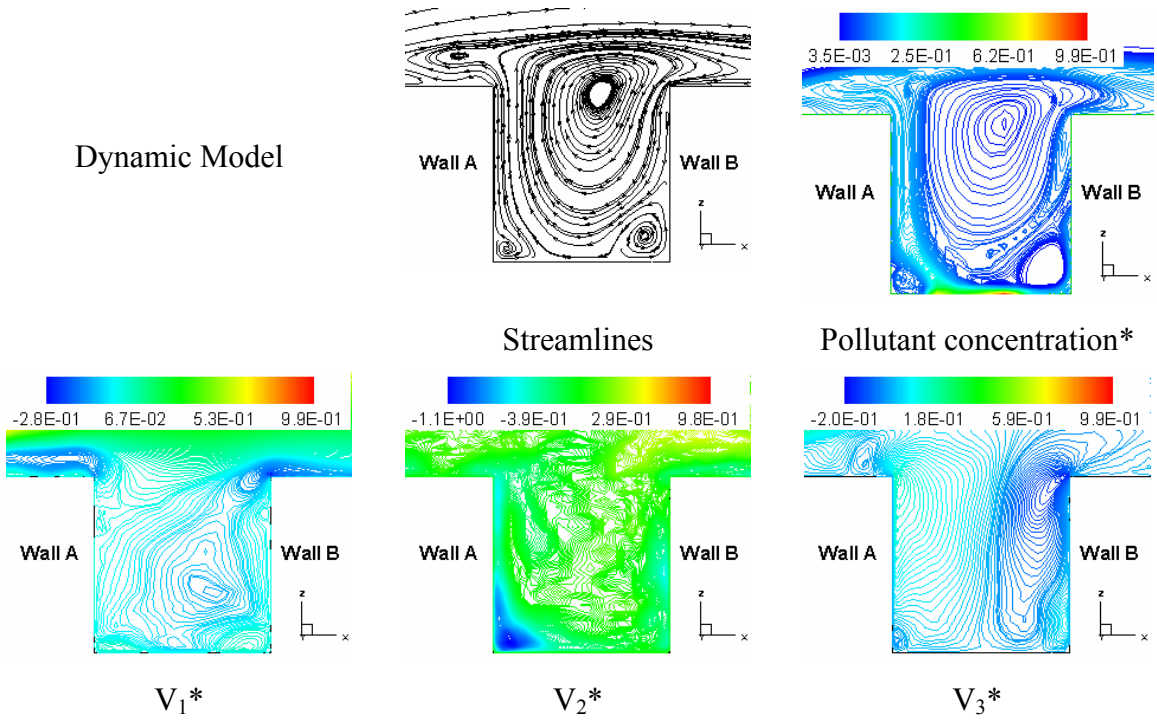


Figure 12. Three-dimensional street canyon: time average fields on plane y = 60 m – streamlines, normalized pollutant concentration and normalized velocity components V1, V2 and V3.

Pollutant concentration contours on the canyon leeward (wall A) and windward (wall B) walls are presented in Fig. 13. By analyzing Fig. 13 one can observe that the average concentration values on wall A are higher than those obtained on wall B, which can be easily explained by regarding the flow regime inside and above the street canyon. Gromke and Ruck (2007) and Salim et al. (2011) also obtained higher pollutant concentration on wall A, as one can see the Fig. 13 (c).

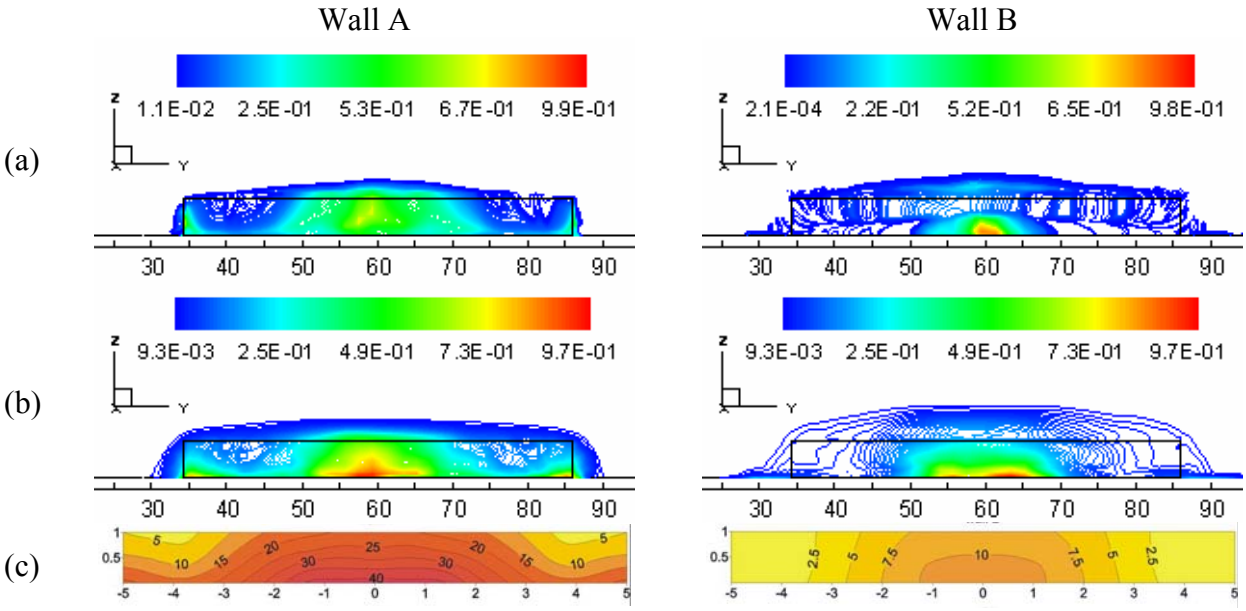


Figure 13. Three-dimensional street canyon: time average fields of pollutant concentration on wall A (x = 30 m) and wall B (x = 35 m): (a) classical model; (b) dynamic model; (c) experimental results from © CODASC, KIT. www.codasc.de

Fig. 14 presents concentration profiles obtained on the center plane of the computational domain (y = 60 m) considering the leeward wall (wall A) and the windward wall (wall B). The present results were obtained using the classical and dynamic SGS models adopted in this work. Comparisons are performed taking into account the experimental work carried out by Gromke and Ruck (2007). According to the results shown, one can see that the concentration distribution along wall A obtained with the dynamic model is very similar to that obtained by wind tunnel experiments. On the other hand, results obtained with the classical model differ mainly in the lower region due to the vortex formed in that region, which is slightly bigger than the one observed from predictions obtained when the dynamic model is employed. With respect to the results obtained along wall B, differences between numerical and experimental results can be noted. The numerical simulations performed in this work led to higher concentration levels in the lower region of the cavity due to the pronounced vortex formed in this corner, which maintains the pollutant near the bottom of the street canyon.

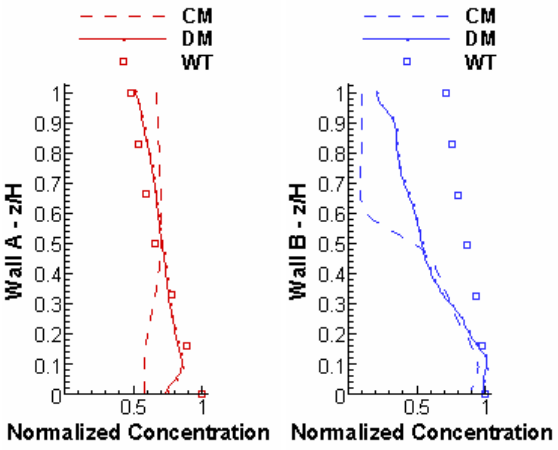


Figure 14. Three-dimensional street canyon: mean concentration profiles on wall A and wall B using the classical model (CM), the dynamic model (DM) and experimental results obtained in a wind tunnel (WT).

Figure 15 shows time-averaged streamlines obtained from the present simulations, where the flow fields correspond to four different positions along the street canyon axis. Considering the flow field above the street canyon and the planes $y^*/H = \pm 0.0, \pm 0.1$ and $\pm 0.3$, the vertical velocity component shows zones where air is coming out or entering the canyon. An ascendant vertical velocity in the first half ($-0.5 \leq x^*/H \leq 0$) and a descendent vertical velocity in the second half ($0 \leq x^*/H \leq 0.5$) is identifiable in these mean streamline fields, where $x^*$ represents the distance in the x direction from the center of the street canyon. However, at position $y^*/H = \pm 0.5$ (lateral edge) the flow above the roof top shows consistently a descendent vertical velocity. Due to superposition by corner eddies the flow field becomes more three dimensional and the canyon vortex is no longer the solely acting flow phenomenon. This behavior was also observed by Gromke and Ruck (2007).

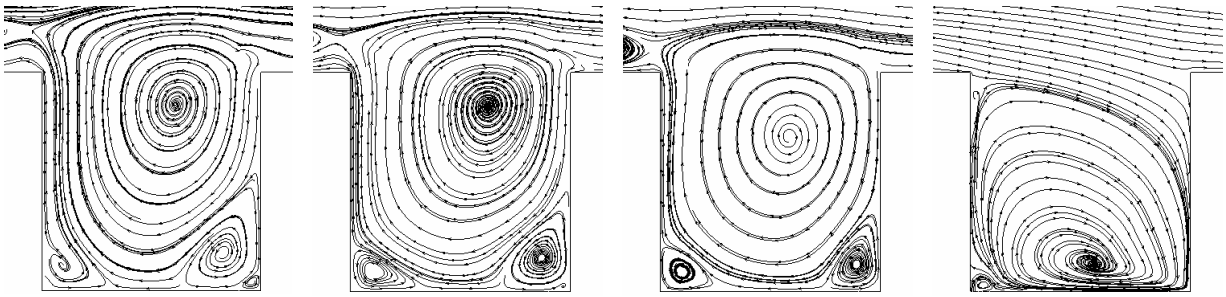

y*/H = 0.0 y*/H = ± 0.10 y*/H = ± 0.3 y*/H = ± 0.5

Figure 15. Three-dimensional street canyon time average streamlines at four different y*/H planes, where y* represents the distance along the axis of the canyon with respect to the symmetry plane.

Three-dimensional time-averaged streamlines obtained in the present analysis are shown in Fig. 16. Flow phenomena such as the horseshoe vortices can be observed in Fig. 16 (a). In Fig. 16 (a) and Fig. 16 (b) one can see streamlines coming from the main flow and entering in the street canyon region through the lateral ends. These phenomena can be only reproduced when three-dimensional models are utilized, justifying the differences observed between results obtained with two and three-dimensional models. Fig. 16 (c) presents streamlines along height, where recirculation zones and stationary vortices can be identified.

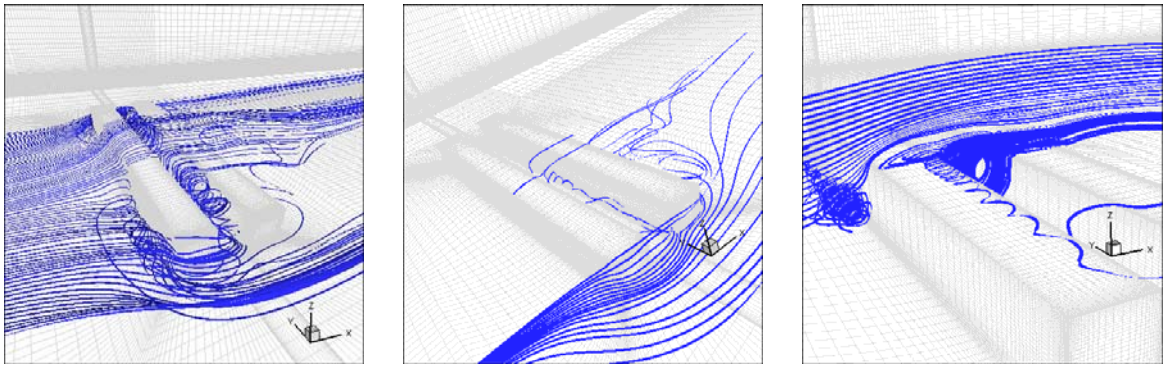

(a) (b) (c)

Figure 16. Three-dimensional street canyon: time average streamlines at z=1 m (a); at y=40 (b); at y=60m (c).

Considering the two-dimensional modeling, two analyses were carried out. In the first analysis all the same parameters employed in the three-dimensional modeling were reproduced, where Cs= 0.12. In the second analysis, only the Smagorinsky's constant was modified, which was considered equal to 0.06. Fig 17 presents the time average results obtained in the first and in the second analysis. Considering the time average streamlines obtained for the first analysis (see Fig. 17 (a)), one can notice a primary counterclockwise vortex and smaller vortices at the corners of the canyon. In this case, the streamlines passing through the first building detach and reattach along the top surface of the second building, near the downstream edge, forming a clockwise recirculation zone above the canyon cavity, which leads to a counterclockwise circulation inside the canyon. Notice that in the 3d modeling there is a clockwise main recirculation inside the canyon. However, the recirculations obtained before the upstream building and after the downstream building are similar to those obtained when the three-dimensional model is employed. On the other hand, in the second analysis (see Fig. 17 (b)), the streamlines passing through the first building detach and reattach along the top surface of the second building, near the upstream edge,

forming a clockwise recirculation zone which enters in the canyon cavity, leading to a clockwise circulation in this region. Considering results of the three-dimensional modeling for the classical model, where a clockwise main recirculation is also obtained (see Fig. 12 or Fig. 15 for y*/H = 0.0) one can see that the vortex center is slightly shifted to the right in the three-dimensional case. Moreover, secondary recirculation located in the bottom corners present equivalent magnitudes if compared with three-dimensional results. As observed before, the pollutant concentration tends to follow the main recirculation of the street canyon and in this sense, one can visualize a major pollutant concentration along the windward wall for the first case, where a counterclockwise main recirculation is formed inside the canyon. In addition, a major pollutant concentration along the leeward wall can be identified in the second case, where a clockwise main recirculation is formed. Additional two-dimensional tests considering a mesh refined twice more than the first configuration were performed and similar results were obtained.

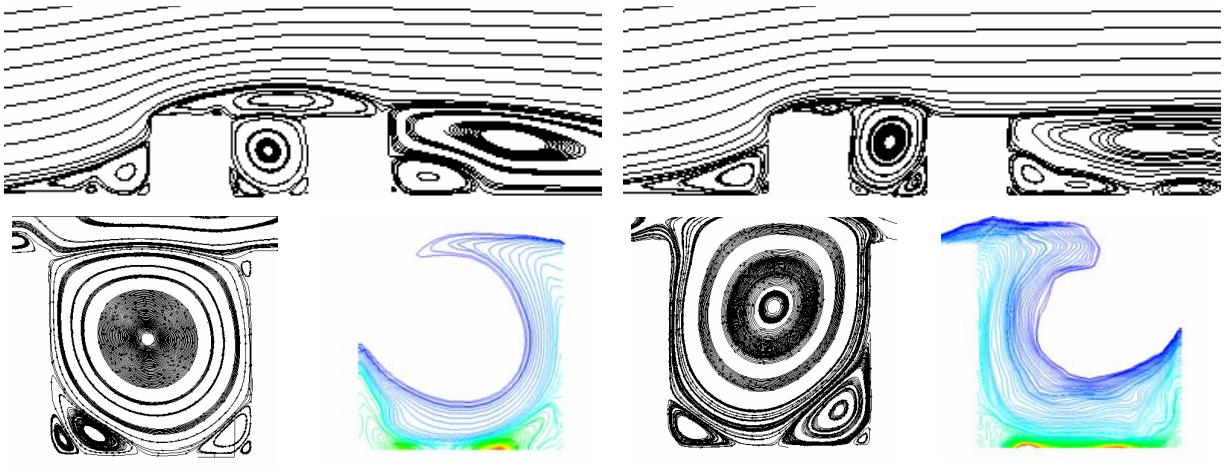

(a) (b)

Figure 17. Two-dimensional street canyon: time-averaged streamlines and pollutant concentration for Cs = 0.12 (a) and Cs = 0.06 (b).

## 5 EFFICIENCY EVALUATION OF THE PARALLEL CODE

Information about the required CPU time for the numerical applications performed in the present work are summarized in Table 3. Furthermore, the Speed-up (Sp) and Efficiency (Ep) curves obtained in the present study, considering a finite element mesh with 1326950 elements, are shown in Fig. 18.

| | **Number of elements** | **CPU time [hours]** | **Total number of steeps** |
|---|---|---|---|
| **Urban Area 3D (Numerical Application 4.1)** | 1268272 | 104.334 | 2.50E+05 |
| **Street Canyon 3D (Numerical Application 4.2)** | 1326950 | 999.602 | 2.00E+06 |

Table 3. CPU time information for some numerical applications.

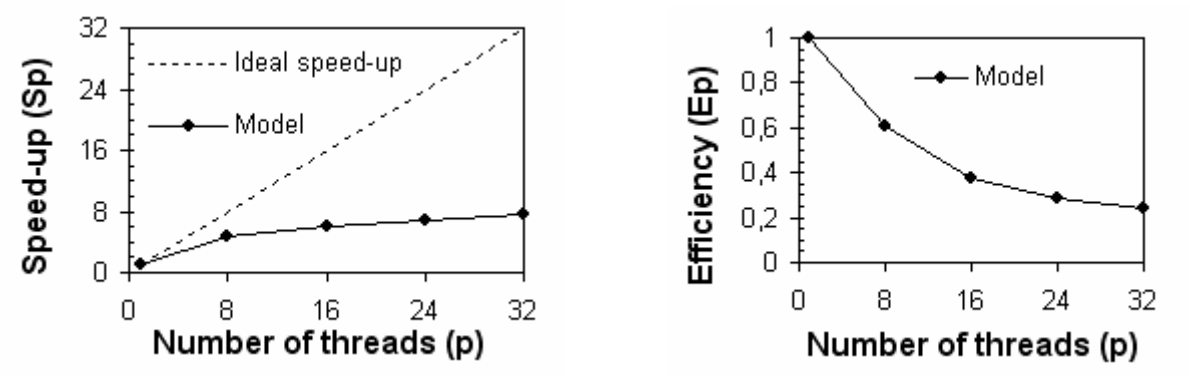


Figure 18. Computational performance obtained by the parallelization scheme utilized in this work. Speed-up: Sp = T1/Tp, T1 – execution time corresponding to the sequential algorithm; Tp – execution time corresponding to the parallel algorithm with p threads; Efficiency: Ep = Sp/p.

## 6 CONCLUSIONS

A numerical model to investigate urban street canyon flows was presented in this work, where a finite element formulation using eight-node hexahedral elements with one-point quadrature and LES was considered. The model proposed by Braun and Awruch (2009a) for investigations on building aerodynamics was extended here to deal with problems of heat and mass transport in the urban microscale. In the present model, the governing equations for incompressible flows with heat and mass transfer were formulated taking into account the pseudo-compressibility hypothesis in order to evaluate explicitly the pressure field and employing LES for turbulence simulation. The present model was validated using a two-dimensional street canyon model investigated previously by Meroney et al. (1996) and Pavageau and Schatzmann (1999) and the cavity flow problem under isothermal and non-isothermal conditions, which was numerically investigated by Ghia et al. (1982) and Agrawal et al. (2001), characterizing the flow conditions usually found in urban street canyons.

In order to verify the relevance of the modeling dimensionality in a pollutant dispersion investigation, two numerical applications were studied considering two and three-dimensional models. In the realistic problem proposed, where an urban region was reproduced considering a typical geometric configuration found in large cities, and in the urban street canyon problem three-dimensional flow structures, with some characteristics which are not observed in two-dimensional models, were simulated. These flow structures affect the pollutant removal, highlighting the relevance of the model dimensionality in a pollutant dispersion investigation. In this sense, numerical investigations of street canyon considering two-dimensional models are justified only to represent flows in street canyons with infinite length along the span-wise direction. Although computational efforts are significantly reduced when two-dimensional simulations are carried out, some flow phenomena such as horseshoe vortices and lateral eddy circulation associated with wake and interference flows cannot be reproduced when the two-dimensional approach is adopted. These flow structures play an important role in pollutant dispersion around buildings and, therefore, reliable analysis of flow and transport problems require three-dimensional models. The three-dimensional street canyon configuration investigated in this work (W/H = 1; L/H = 10), for instance, cannot be analyzed considering a two-dimensional model, since three-dimensional flow phenomena were observed and modified the flow field inside the canyon cavity. According to results obtained from two-dimensional simulations, the pollutant emitted from the bottom of the canyon can be only removed through the top of the canyon. On the other hand, a three-dimensional model

indicates that the pollutant is also removed through the lateral ends of the canyon, due to the occurrence of a suction zone induced by the outer flow. Considering the SGS models employed, in most of the applications analyzed here, predictions obtained with the dynamic and classical models presented similar results.

A good performance was obtained in the efficiency evaluation of the parallelization technique adopted in this work. For future works, a model considering chemical reactions should be implemented in order to improve the numerical description of the physical phenomena in problems where their time scales are comparable to time scales of pollutant transport. In addition, high emission sources of pollutants such as those associated with stacks or canopies should be also analyzed.

## REFERENCES

Agrawal, L., Mandal, J. C., and Marathe, A. G. Computations of laminar and turbulent mixed convection in a driven cavity using pseudo-compressibility approach. *Computers & Fluids*, 30: 607-620, 2001.

Ahmad, K., Khare, M., Chaudhry, K.K. Wind tunnel simulation studies on dispersion at urban street canyons and intersections: a review. *Journal of Wind Engineering and Industrial Aerodynamics*, 93: 697-717, 2005.

Assimakopoulos, V. D. A., Simon, H. M., Moussiopoulos, N. A numerical study of atmospheric pollutant dispersion in different two-dimensional street canyon configurations. *Atmospheric Environment*, 37: 4037-4049, 2003.

Baik, J.-J., Kim, J.-J. A numerical study of flow and pollutant dispersion characteristics in urban street canyons. *Journal of Applied Meteorology*, 38: 1576-1589, 1999.

Baik, J.-J., Kim, J.-J., Fernando, H.J.S. A CFD model for simulating urban flow and dispersion. *Journal of Applied Meteorology*, 42: 1636-1648, 2003.

Braun, A.L., Awruch, A.M. Aerodynamic and aeroelastic analyses on the CAARC standard tall building model using numerical simulation. *Computers and Structures*, 87: 564-581, 2009a.

Braun, A.L., Awruch, A.M. An energy-conserving partitioned model for fluid-structure interaction problems using hexahedral finite elements with one-point quadrature. International Journal for Numerical Methods in Engineering, 79: 505-549, 2009b.

Chan, A.T., Au, W.T.W., So, E.S.P. Strategic guidelines for street canyon geometry to achieve sustainable street air quality. Part II: multiple canopies and canyons. *Atmospheric Environment*, 37: 2761-2772, 2003.

Chan, T.L., Dong, G., Leung, C.W., Cheung, C.S., Hung, W.T. Validation of a two-dimensional pollutant dispersion model in an isolated street canyon. *Atmospheric Environment*, 36: 861-872, 2002.

Cheng, W.C., Liu, C-H. Large-eddy simulation of turbulent transports in urban street canyons in different thermal stabilities. *Journal of Wind Engineering and Industrial Aerodyanmics*, 99: 434-442, 2011.

Germano, M., Piomelli, U., Moin, P., Cabot, W.H. A dynamic subgrid-scale eddy viscosity model. *Physics of Fluids*, A3: 1760-1765, 1991.

Ghia, U., Ghia, K.N., Shin, C.T. High-Re Solutions for Incompressible Flow Using the Navier-Stokes Equations and a Multigrid Method. *Journal of Computational Physics*, 48: 387-411, 1982.

Gromke C, Ruck B. Influence of trees on the dispersion of pollutants in an urban street canyon— Experimental investigation of the flow and concentration field. *Atmospheric. Environment*, 41:3287–3302, 2007.

Gromke C, Ruck B. On the impact of trees on dispersion processes of traffic emissions in street canyons. *Boundary-Layer Meteorology*, 131:19–34, 2009.

Gromke C, Ruck B. Pollutant Concentrations in Street Canyons of Different Aspect Ratio with Avenues of Trees for VariousWind Directions. *Boundary-Layer Meteorology*, 144:41–64, 2012.

Hajra, B. Recent studies in CFD modelling of pollutant dispersion in street canyons. *Building Simulation*, available online: 1-12, 2011.

Jeong, S. J., Andrews, M.J. Application of the k-ε turbulence model to the high Reynolds number skimming flow field of an urban street canyon. *Atmospheric Enviroment*, 36: 1137-1145, 2002.

Kim, J-J and Baik, J-J. A numerical study of thermal effects on flow and pollutant dispersion in urban street canyons. Journal of Applied Meteorology, 38: 1249-1261, 1999.

Lee, I.Y., Park, H.M. Parameterization of the pollutant transport and dispersion in urban street canyons. *Atmospheric Environment,* 28: 2343-2349, 1994.

Li, X.X., Koh, T.Y., Britter, R., Liu, C.H., Norford, L.K., Entekhabi, D., Leung, D.Y.C. Large-eddy simulation of flow field and pollutant dispersion in urban street canyons under unstable stratification. In: Proceeding of the 7th International Conference on Urban Climate (ICUC-7), Yokohama, Japan, 2009.

Li, X.X., Liu, C.H., Leung, D.Y.C., Lam, K.M. Recent progress in CFD modelling of a wind field and pollutant transport in street canyons. *Atmospheric Environment*, 40: 5640-5658, 2006.

Lilly, D.K. A proposed modification of the Germano subgrid-scale closure method. *Physics of Fluids*, 4: 633-635, 1992.

Meroney, R.N, Pavageau, M., Rafailidis, S., Schatzmann, M. Study of line source characteristics for 2-D physical modelling of pollutant dispersion in street canyons. In: *Journal of Wind Engineering and Industrial Aerodynamics*, 62: 37–56, 1996.

Oke, T. R. Street design and urban canopy layer climate. *Energy and Buildings*, 11: 103-113, 1988.

Pavageau, M., Schatzmann, M. Wind tunnel measurements of concentration fluctuations in an urban street canyon. *Atmospheric Environment*; 33: 3961-3971, 1999.

Salim S. M., Cheah S. C., Chan A. Numerical simulation of dispersion in urban street canyons with avenue-like tree plantings: Comparison between RANS and LES. *Build and Environment*, 46:1735–1746, 2011.

Sini, J.-F., Anquetin, S., Mestayer, P.G. Pollutant dispersion and thermal effects in urban street canyons. *Atmospheric Environment,* 30: 2659-2677, 1996.

Smagorinsky, J. General circulation experiments with the primitive equations I. The basic experiment. *Monthly Weather Review*, 91: 99-164, 1963.

Soulhac, L., Garbero, V., Salizzoni, P., Mejean, P., Perkins, R.J. Flow and dispersion in street canyons. *Atmospheric Environment*, 43: 2981-2996, 2009.

Stathopoulos, T., Baskaran, A. Computer simulation of wind environmental conditions around buildings. *Engineering Structures*, 18: 876-885, 1996.

Vardoulakis, S., Fisher, B.E., Pericleous, K., Gonzalez-Flesca, N. Modelling air quality in street canyons: A review. *Atmospheric Environment*, 37: 155-182, 2003.

Xie, X., Huang, Z., Wang, J., Xie, Z. The impact of solar radiation and street layout on pollutant dispersion in street canyon. *Building and Environment*, 40: 201-212, 2005.

Xie, X., Liu, C-H., Leung, D.Y.C., Leung, M.K.H. Spatial distribution of traffic-related pollutant concentrations in street canyons. *Atmospheric Environment*, 40: 6396-6409, 2006.

Yassin, M.F., Kellnerová, R., Janour, Z. Impact of street intersections on air quality in urban

environment. *Atmospheric Environment*, 42: 4984-4963, 2008.